Journal of Colloid and Interface Science 678 (2025) 766–775

Contents lists available at ScienceDirect

Journal of Colloid And Interface Science

journal homepage: www.elsevier.com/locate/jcis

Regular Article

Design of innovative and low-cost dopamine-biotin conjugate sensor for the efficient detection of protein and cancer cells

Monica Notarbartolo [a], Maria Laura Alfieri [b,*], Roberto Avolio [c], Vincent Ball [d,e], Maria Emanuela Errico [c], Marina Massaro [a,*], Roberta Puglisi [f], Rita Sànchez-Espejo [g], César Viseras [g,h], Serena Riela [f]

[a] Dipartimento di Scienze e Tecnologie Biologiche, Chimiche e Farmaceutiche (STEBICEF), Università di Palermo, Viale delle Scienze, Parco d'Orleans II, Ed. 16-17, 90128 Palermo, Italy
[b] Department of Chemical Sciences, University of Naples "Federico II", I-80126 Naples, Italy
[c] Institute of Chemistry and Technology of Polymers, National Council of Research (CNR), via Campi Flegrei 34, Pozzuoli I-80078, Italy
[d] Université de Strasbourg, Faculté de Chirurgie Dentaire, 8 rue Sainte Elizabeth, 67000 Strasbourg. France
[e] Institut National de la Santé et de la Recherche Médicale, Unité mixte de rechere 1121. 1 rue Eugène Boeckel, 67084 Strasbourg Cedex, France
[f] Dipartimento di Scienze Chimiche (DSC), Università di Catania, Viale Andrea Doria 6, 95125 Catania, Italy
[g] Department of Pharmacy and Pharmaceutical Technology, Faculty of Pharmacy, University of Granada, Campus Universitario de Cartuja, 18071 Granada, Spain
[h] Andalusian Institute of Earth Sciences, CSIC-UGR, 18100 Armilla, Granada, Spain

GRAPHICAL ABSTRACT

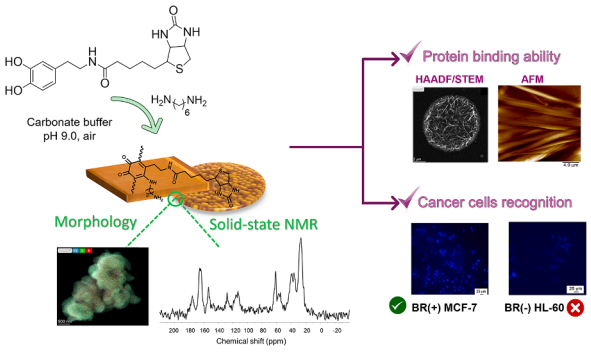

ARTICLE INFO

Keywords:
Dopamine
Biotin
Dip-coating
Low-cost sensor
Avidin
HL-60 and MCF-7 cells

ABSTRACT

The rapid, precise identification and quantification of specific biomarkers, toxins, or pathogens is currently a key strategy for achieving more efficient diagnoses. Herein a dopamine-biotin monomer was synthetized and oxidized in the presence of hexamethylenediamine, to obtain adhesive coatings based on polydopamine-biotin (PDA-BT) on different materials to be used in targeted molecular therapy. Insight into the structure of the PDA-BT coating was obtained by solid-state ^{13}C NMR spectroscopy acquired, for the first time, directly onto the coating, deposited on alumina spheres. The receptor binding capacity of the PDA-BT coating toward 4-

Abbreviations: HMDA, hexamethylenediamine; HAADF/STEM, high angle annular dark field scanning transmission microscopy; AFM, atomic force microscopy; HABA, 4-hydroxyazobenzene-2-carboxylic acid; EDC, 1-ethyl-3-(3-dimethylaminopropyl)-carbodiimide; TEM, transmission electron microscopy.

* Corresponding authors.
E-mail addresses: marialaura.alfieri@unina.it (M.L. Alfieri), marina.massaro@unipa.it (M. Massaro).

https://doi.org/10.1016/j.jcis.2024.09.145
Received 13 June 2024; Received in revised form 30 August 2024; Accepted 15 September 2024
Available online 18 September 2024

hydroxyazobenzene-2-carboxylic acid/Avidin complex was verified by means of UV–*vis* spectroscopy. Different deposition cycles of avidin onto the PDA-BT coating by layer-by-layer assembly showed that the film retains its receptor binding capacity for at least eight consecutive cycles. Finally, the feasibility of PDA-BT coating to recognize cell lines with different grade of overexpression of biotin receptors (BR) was investigated by tumor cell capture experiments by using MCF-7 (BR+) and HL-60 (BR−) cell lines. The results show that the developed system can selectively capture MCF-7 cells indicating that it could represent a first approach for the development of future more sophisticated biosensors easily accessible, low cost and recyclable with the dual and rapid detection of both proteins and cells.

1. Introduction

The rapid, precise identification and quantification of specific biomarkers, toxins, or pathogens is currently a key strategy for achieving more efficient diagnoses. Targeted molecular therapy could perform for example release of anticancer drugs, specifically identify overexpressed natural receptors on the cancer cell, and achieve targeted killing of tumor cells [1].

Current technology platforms for the simultaneous capture and identification of circulating tumor cells, cells that detach from solid primary tumors during metastasis, involve immunomagnetic beads, microfluidic devices, a lot of inorganic or organic materials (*e.g.*, silica and titanium dioxide nanospheres or nanofibers, graphene oxide nanoplates, silicon nanowires and polymer nanostructures) as well as nanostructures conjugated with antibodies [2–12]. However, the clinical applications of these materials suffer several disadvantages related to the high cost of synthetic materials, the difficulty of creating nanostructures, the device's poor reproducibility, the low capture specificity, and the high price of the graft antibody [13–18].

Among the cancer-targeting units, biotin has recently drawn much attention due to its low molecular weight, relatively simple biochemical structure, low cytotoxicity, absence of antigenicity and immunogenicity and high tumor specificity [19–24]. In fact, biotin proved to be an ideal targeted ligand for various anti-cancer drugs since its receptor are over expressed on numerous cancer cells, characterized by rapid dividing and aggressive growth, as opposed to healthy cells where the receptors are hardly ever expressed [25–28]. In addition, biotin has a strong affinity and specificity for avidin and streptavidin (its bacterial counterpart), through noncovalent bonds, and relatively low immune response *in vivo*, which facilitate the receptor-mediated endocytosis of biotinylated nanoparticles in cancer cells and therefore represent an attractive choice for target specific diagnostic and theranostic studies [21,25,29–32]. In this regard, the development of biotin-avidin technologies has raised much attention because of both the avidin–biotin unparalleled binding properties to various biomaterials (*e.g.,* DNA/RNA, NPs, antibodies, and aptamers) and the interaction is a useful tool for surface modification of materials as a rapid screening platform [33–41].

Polydopamine (PDA), a melanin-like pigment that derives from the oxidative polymerization of dopamine under mild alkaline conditions, has recently attracted intense research in biomedical field for sensing applications due to the simplicity of its synthesis, versatility, biocompatibility and more importantly its universal substrate-independent coating properties [42–45].

Dopamine molecules, featuring a catechol unit and a primary amine side chain, also provide an effective means of secondary functionalization with either polymers, metallic nanoparticles or biomolecules (such as proteins, nucleotides, oligosaccharides and lipids). Furthermore, the surface modification of PDA coated materials is facile affording thus new biohybrid materials for diverse applications [45–51]. Most of the biomolecules can interact with PDA through hydrogen bonding, π–π stacking, cation–π and electrostatic attraction interactions as well as *via* covalent grafting by means of thiol or amino groups for specific recognition [52–55].

Some of the recent examples in this field include for example the deposition of PDA on cancer cell membranes to facilitate targeted delivery of anticancer drugs [56–58], the targeting transmembrane MUC18, a tumor progression marker, with polydopamine nanoparticles as well as the sensitive detection of HeLa and HL-60 cells by specific recognition of a polydopamine-coated carbon nanotubes–folate nanoprobe to cell-surface folate receptors [59,60].

In addition, a previous finding suggested also that the functionalization of the outer surface of halloysite nanotubes with PDA represents a suitable anchoring point for the grafting of biotin, followed by avidin binding, for further developments in theranostics and bioimaging for cancer treatment [61].

Based on these premises, herein, we merge the unique adhesive properties of dopamine precursor with the receptor-binding capability of biotin to develop, for the first time to the best of our knowledge, easily accessible, low cost, and recyclable biosensors with the dual and rapid detection of both proteins and tumor cells. To this aim, a *N*-biotinyl-(3,4-dihydroxyphenylethylamide) (DA-BT) was simply prepared through amide bond formation by EDC mediated condensation between dopamine and biotin. Afterwards, its oxidation in the presence of hexamethylenediamine (HMDA), a long aliphatic chain diamine, provides the basis for the design of an innovative, and simple dip-coating methodology to achieve a biocompatible organic thin film (PDA-BT) which can adhere to a broad range of surfaces. The coated surface was characterized from the chemical and morphological standpoints and its receptor-binding ability toward the 4-hydroxyazobenzene-2-carboxylic acid (HABA)/Avidin complex was investigated as well as the capture of tumor cells.

The development of PDA-biotin technology could represent an attractive choice for potential applications in different areas of material functionalization, biomedical imaging and pharmacology (*e.g.*, cell imaging, bio-species sensing, prodrug designing, and tumor therapy).

2. Materials and methods

Dopamine hydrochloride, biotin, 1-ethyl-3-(3-dimethylaminopropyl)-carbodiimide (EDC), HMDA, HABA/Avidin reagent (lyophilized powder, MQ200) and Avidin from egg white were purchased from Sigma Aldrich (Merck, Milan, Italy) and used without any further purification.

Quartz or glass substrates were cleaned by soaking in a piranha solution (96 % H_2SO_4/30 % H_2O_2 5:1 v/v) overnight, rinsed with distilled water and dried under vacuum.

UV–*vis* spectra were recorded on a Jasco V-730 Spectrophotometer.

Solid-state NMR experiments were performed on a Bruker Avance II 400 spectrometer equipped with a 4 mm MAS probe. Alumine oxide coated particles were packed into 4 mm zirconia rotors sealed with Kel-F caps. ^{13}C CP-MAS spectra were acquired with a variable spin-lock sequence and a contact time of 2 ms, using a ^{1}H $\pi/2$ pulse width of 3.8 μs and a relaxation delay of 4 s. The spinning speed was set at 9 kHz and 20,000 scans were recorded.

Transmission Electron Microscopy (TEM) was performed by means of a FEI Titan G2 60-300 ultra-high resolution transmission electron microscope coupled with Analytical Electron Microscopy (AEM) performed with a SUPER-X silicon-drift windowless X-ray Energy-Dispersive Spectroscopy (XEDS) detector. AEM spectra were saved in mode STEM (Scanning Transmission Electron Microscopy) with a

HAADF (High Angle Annular Dark Field) detector. X-ray chemical element maps were also collected.

The film morphology of the investigated films was characterized by AFM using a Catalyst AFM microscope (Bruker Inc, Santa Barbara, CA, USA). The images were acquired at a frequency of 0.5 Hz in the scan assist mode and in the dry state within regions of interest (5 μm × 5 μm or 20 μm × 20 μm) and with a resolution of 512 × 512 pixels. The used cantilevers had a spring constant of 0.7 $N.m^{-1}$ as given by the furnisher (Bruker Inc, Santa Barbara, CA, USA).

The static contact angles of small water droplets (5 μL) were measured on the investigated films with an Attension Theta goniometer (Biolin Scientific, Vastra Frolunda, Sweden) and the given values correspond to the average (±one standard deviation) over three deposited droplets.

2.1. Synthesis of N-biotinyl-(3,4-dihydroxyphenylethylamide) (DA-BT)

In a round bottom flask, biotin (2 g, 8.9 mmol, 1 eq) and EDC·HCl (1.92 g, 10 mmol, 1.12 eq) were weighed and anhydrous DMF (80 mL) was added. The obtained solution was left under stirring at room temperature for 10 min. Afterwards, to this, a solution of dopamine HCl (3.95 g, 20 mmol, 2.24 eq) and pyridine (3.20 mL, 40 mmol, 4.5 eq) in anhydrous DMF (40 mL) was added dropwise. The mixture was left to stir at r.t. overnight. Then the solvent was evacuated and the obtained solid was purified by chromatographic column using CH_2Cl_2/MeOH (10:1) as eluent. DA-BT compound was obtained as a white powder with a yield of 45 %. The identity and purity were confirmed by ^1H and ^{13}C NMR analysis (Figs. S1 and S2).

^1H NMR (300 MHz, CD_3OD) δ (ppm): 1.34–1.39 (m, 2H, C**H**$_2$), 1.59–1.65 (m, 4H, C**H**$_2$), 2.17–2.20 (t, 2H, C**H**$_2$), 2.63–2.68 (t, 2H, C**H**$_2$), 2.93–3.00 (dd, 1H, C**H**), 3.16–3.19 (m, 1H, C**H**), 3.33–3.39 (m, 3H, C**H**$_2$ and C**H**), 4.29–4.32 (m, 1H, C**H**), 4.49–4.52 (m, 1H, C**H**), 6.55–6.56 (d, 1H, Ar-C**H**), 6.65–6.71 (t, 2H, C**H**).

^{13}C NMR (300 MHz, CD_3OD) δ (ppm): 25.10, 28.01, 33.98, 35.39, 39.57, 40.46, 55.49, 60.22, 61.92, 105.67, 114.94, 115.51, 119.66, 130.61, 143.34, 144.81, 174.58, 207.37.

2.2. General procedure for substrate coating (PDA-BT)

DA-BT was dissolved in the minimal amount of methanol and added to a solution of HMDA in 0.05 M sodium carbonate buffer pH=9.0 to final concentrations in the range of 1–10 mM, at a catechol/amine molar ratio of 1:1 and the mixture was taken under vigorous stirring. Quartz or glass substrates were dipped into the reaction mixture and left under stirring for 24 h, then rinsed with distilled water, sonicated in methanol/water solution 1:1 v/v in an ultrasonic bath, air-dried and analyzed by UV–*vis* spectrophotometry. Coating of other materials including polycarbonate and aluminum oxide was run under the same conditions.

2.3. Interaction with HABA/Avidin

The PDA-BT coated glass substrates were immersed in a stock solution of HABA/Avidin reagent in deionized water (1 mL) and the receptor-binding capacity was evaluated by UV–*vis* spectroscopy measuring the absorbance of HABA/Avidin at 500 nm over 1 h.

2.3.1. Calculation of biotin adhered on the surface

The amount of biotin in the coated sample was determined as follows:

$$\Delta A_{500} = 0.9 \cdot A_{550}\ \text{HABA/Avidin} + A_{500}\ \text{sample blank} - A_{500}\ \text{HABA/Avidin} + \text{sample} \quad (1)$$

where 0.9 is the dilution factor of HABA/Avidin upon addition of sample, A_{550} HABA/Avidin, A_{500} sample blank and A_{500} HABA/Avidin + sample are the absorbance of the HABA/Avidin reagent solution, the PDA-BT coating dissolved in DMSO and the HABA/Avidin reagent dispersion in the presence of PDA-BT solution at 500 nm.

$$[\text{Biotin}]\ (\mu M) = (\Delta A\_500)/34 \cdot 10 \quad (2)$$

where 34 is the μM extinction coefficient at 500 nm and 10 is the dilution factor of the sample into the cuvette.

2.3.2. Layer-by-layer Avidin-biotin deposition

PDA-BT (10 mM) coatings were dipped in 1 mL HABA/Avidin solution for 1 h. The substrates were then rinsed with distilled water, air dried and dipped in a 50 mM biotin solution in distilled water. After 30 min the substrates were rinsed with distilled water and air dried. The two sequential assembly steps were repeated four times. Aliquots of the medium were withdrawn periodically and analyzed spectrophotometrically measuring the HABA/Avidin absorption peak at 505 nm.

2.4. Cell culture and capture experiment

HL-60 cells were cultured in Roswell Park Memorial Institute (RPMI) 1640, while MCF-7 cells were cultured in Dulbecco's Modified Eagle Medium (DMEM) (HyClone Europe Ltd., Cramlington, UK) supplemented with 10 % heat inactivated fetal calf serum, 2 mM L-glutamine, 100 units/mL penicillin and 100 μg/mL streptomycin (all reagents were from HyClone Europe Ltd., Cramlington, UK) in a humidified atmosphere at 37 °C in 5 % CO_2. HL-60 and MCF-7 cells were obtained from ATCC®, cells from both cell lines were seeded on glass slides at the density of 5000 cells/well in a final volume of 200 μL of complete medium without serum, to avoid a possible interference on the adhesion processes of factors contained in the serum, and incubated overnight at 37 °C in a humidified 5 % CO_2 atmosphere. After 24 h the cells were washed in 1× PBS for three times and fixed with 4 % formaldehyde for 10 min before washing three times with PBS and nuclei were stained with 1 μg/mL of the nuclear stain DAPI (4′,6-diamidino-2-phenylindole) (Invitrogen) for 10 min. After nuclear staining, cells were further washed with PBS 1× for three times and the slides were observed with an Olympus Fluorescence microscope (Olympus, Japan) using a 20× objective.

2.5. Statistical analysis

The statistical analysis of the experimental data was estimated using the statistical analysis software Past 4.03. The test was performed in duplicate, and the data were analyzed using a one-way analysis of variance (ANOVA). The significant difference values were tested using the Tukey test with a 95 % of confidence interval ($p < 0.05$). The final results were displayed in the form of mean ± standard deviation.

3. Results and discussion

N-Biotinyl-(3,4-dihydroxyphenylethylamide) (DA-BT) was synthetized adapting a procedure reported elsewhere [62]. In details, dopamine hydrochloride (DA) was reacted with biotin (BT) in DMF in the presence of EDC as coupling agent, affording the DA-BT molecule with a yield of 45 % (Scheme 1).

Autoxidation of DA-BT (1 mM, pH 8.5–9.0), in phosphate or bicarbonate buffer didn't result in detectable coatings on glass or quartz, despite apparent polymerization and darkening of the mixture. Therefore, based on preliminary observations indicating that the addition of HMDA enables film deposition with most of catechol [63–66] (including dopamine at very low concentrations) [67] during catechol polymerization, the HMDA-modified dip-coating protocol was extended to the DA-BT. In this procedure, the immersion of quartz substrates into a solution containing DA-BT (1 mM, pH 9.0) in the presence of HMDA (1 mM) resulted in the deposition of a yellowish-orange film (PDA-BT) after 24 h, as detected by UV–*vis* spectroscopy (Fig. 1A). A systematic

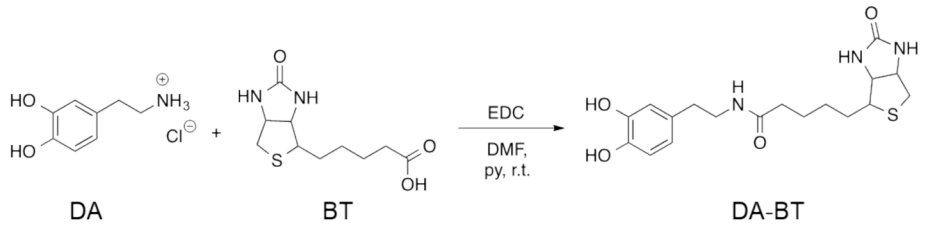

Scheme 1. Schematic synthesis of DA-BT.

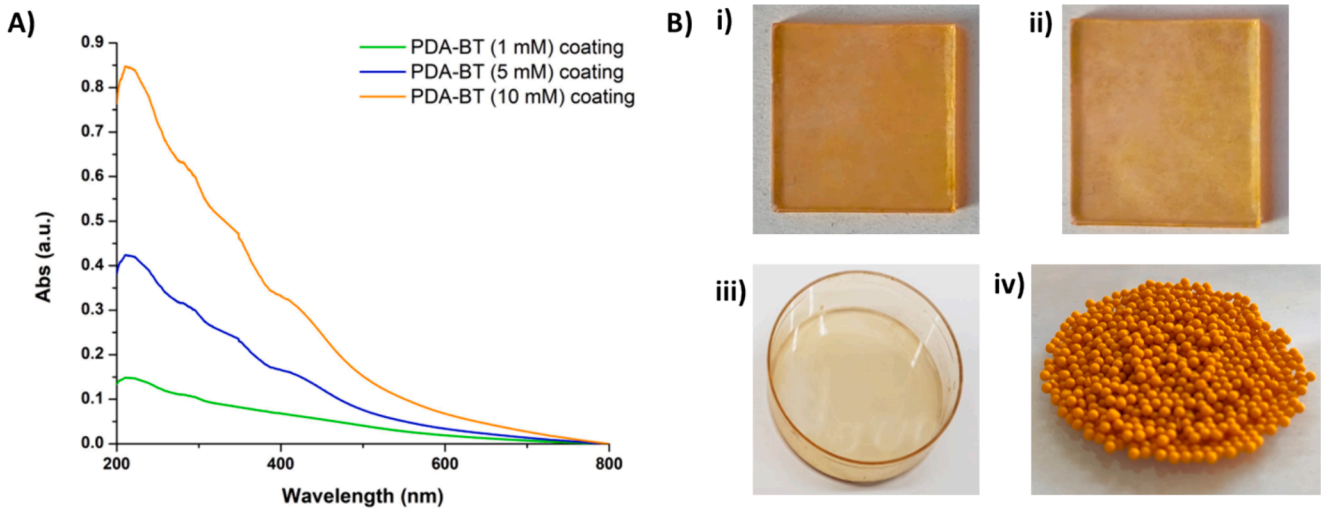

Fig. 1. A) UV–*vis* spectra of quartz slides dipped in DA-BT solutions (in the range 1–10 mM) in 0.05 M carbonate buffer (pH 9.0) in the presence of equimolar amounts of HMDA for 24 h. B) PDA-BT coatings on: i) quartz; ii) glass; iii) polycarbonate; and iv) aluminum oxide.

investigation of the reaction conditions, by increasing the amount of DA-BT/HMDA (Fig. 1A), showed that the maximal film deposition occurs at the concentration of DA-BT/HMDA 10 mM.

Interestingly, the coating was independent of the properties of the surface, indeed efficient film deposition was observed on various materials other than quartz, including plastic surfaces and porous aluminum oxide particles (Fig. 1B).

Insight into the structure of the PDA-BT coating was obtained by solid state ^{13}C NMR analysis.

In this work, ^{13}C solid state NMR spectrum was recorded, for the first time, to the best of our knowledge, directly on PDA-BT coated on porous alumina, chosen as model for its high surface area, rather than on the bulk materials that precipitate during the autoxidation reactions.

As it is possible to note in the ^{13}C solid state NMR spectrum of PDA-BT film, shown in Fig. 2, broad signals in the range 20–40 ppm, attributable to the aliphatic chains of biotin (C1-4), of dopamine-based units (C6, C7) and of HMDA (C1″-C6″), are observable [64]. Furthermore, in the spectrum are clearly observable the signals at *ca.* 55–61 ppm due to carbons C1′-C5′ of biotin; whereas the signals attributable to C3′ and C5 of carboxylic groups of biotin in the low field region are partially superposed with the carbonyl/carboxyl signals of polydopamine.

Based on those evidence it was possible to retrieve some information about the probable structure of the PDA-BT. In particular, the absence of the signals at *ca.*145 ppm, due the C-OH carbons in the catechol ring of DA suggested a high degree of oxidation of DA-BT units during film formation, also confirmed by the increased intensity of the carbonyl/carboxyl peak at *ca.* 170 ppm that indicates a higher conversion of catechol to oxidized quinone groups. Moreover, the aromatic region of the spectrum (110 – 130 ppm) presents two well resolved peaks, in contrast with the complex pattern generally shown by bulk materials that precipitated from the reaction mixtures [64,67]. This would indicate a low level of substitution on the aromatic ring of PDA, suggesting

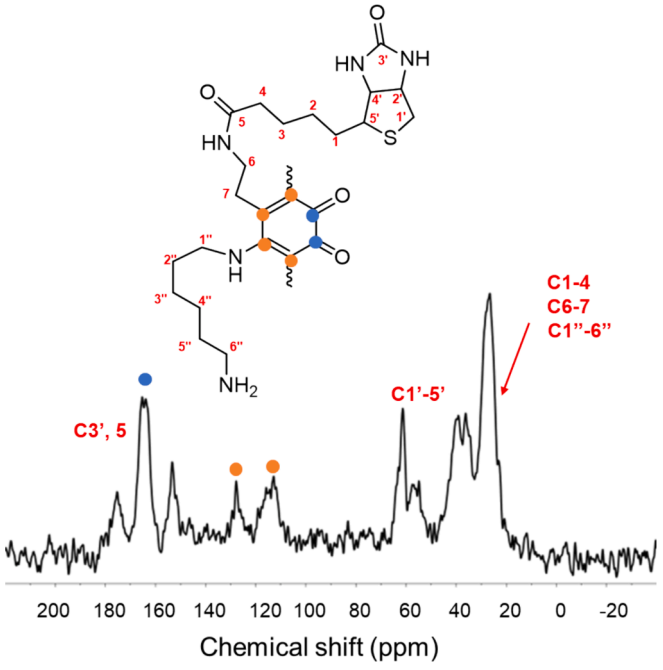

Fig. 2. ^{13}C CP-MAS NMR spectrum recorded on the PDA-BT film deposited onto porous alumina spheres.

that the film is composed of oligomeric species with a relatively low degree of polymerization. Dopamine-quinone could be thus considered as a key branching point in the PDA pathway. In fact, the quinone may be engaged with sequential bimolecular coupling processes of the

dopamine-quinone which would direct the oxidative process toward linear oligomers featuring amide bonds with biotin molecule and giving rise to adhesive cross-linked structures.

The morphology of the PDA-BT coating was imaged by high angle annular dark field Scanning Transmission Microscopy (HAADF/STEM). For this analysis two different films at two different DA-BT initial concentration were considered. In Fig. 3A, for instance, the PDA-BT coating obtained starting from DA-BT 5 mM is shown. As it is possible to observe, the coating consists of round shaped particles with diameters of *ca.* 500 nm. EDX analysis showed the presence of C and N atoms of polydopamine and of S atoms related to the biotin moieties (Fig. 3B). By elemental mapping extrapolated from EDX it was possible to note that the S atoms are uniformly dispersed in the polymer indicating that the biotin, during the polymerization process, arranges itself on the surface of the coating further confirming the NMR results. Similar observations can be drawn for the coating obtained in the case of DA-BT 10 mM (Fig. 3C–D) indicating that the DA-BT initial concentration did not affect the morphology of the final film. However, in this latter case, a more compact morphology was observed in line with the maximum coating achieved in these conditions as observed by the UV–*vis* measurements (Fig. 1A).

A further insight into the surface topography and roughness of the coated sample was obtained by means of Atomic Force Microscopy (AFM) where particles of about the same size as those seen in HAADF/STEM images were observed (Fig. S3).

3.1. Evaluation of the avidin-binding ability

PDA-BT coatings were then investigated for their receptor-binding capacity toward the 4-hydroxyazobenzene-2-carboxylic acid HABA/Avidin complex by means of UV–*vis* spectroscopy. The HABA/Avidin assay was run by dipping the coated substrates (PDA-BT (1 mM), PDA-BT (5 mM), PDA-BT (10 mM)) directly into an aqueous solution of the HABA/Avidin reagent. Aliquots of the medium were then withdrawn periodically and analyzed spectrophotometrically measuring the HABA/Avidin absorption peak at 505 nm. As shown in Fig. 4 and Fig. S4 a progressive decrease in the absorption maximum band of HABA/Avidin complex was observed over time with all types of coated surfaces, consistent with the displacement of HABA molecules from the avidin complex as expected considering the higher association constant for Avidin-Biotin compared to that of HABA/Avidin complex. In particular, the coating prepared starting from the lowest concentration of the DA-BT conjugate that is 1 mM showed lower binding properties leading to a *ca.* 43 % reduction of HABA/Avidin absorption maximum in the first 5 min. Good binding properties have been instead observed for the coating prepared starting from 5 mM DA-BT concentration with a *ca.* 69 % reduction of HABA/Avidin absorption maximum whereas the coating prepared starting from the highest concentration of DA-BT that is 10 mM showed the more efficient binding properties, leading to a *ca.* 87 % reduction of HABA/Avidin absorption maximum in the first 5 min reaching a 94 % reduction after 60 min. The receptor-binding capacity of the polydopamine-biotin coatings is thus proportional to the amount of material deposited on the glass substrate.

Moreover, as shown in Fig. S5, a detectable increase in the film absorbance in the visible region has been observed after one hour dipping in the HABA/Avidin solution further confirming the occurrence of biotin-avidin binding directly on the surface. This assay allowed to estimate the amount of biotin adhered on the surface in the order of 61 μg/cm^2 for glass.

To further prove the interaction of the PDA-BT coating with avidin, the morphology of the nanocomposite treated with HABA/Avidin solution was imaged by HAADF/STEM. The micrographies reported in Fig. 5A–C showed that morphology of the particles changed after interaction with Avidin. As it is possible to observe, the classical round shape of polydopamine is preserved but the particles seem to be aggregated to each other in an organized structure. This morphology could arise from the interaction of the different biotin molecules present at the surface of the coating and avidin (Fig. 5E). From a microscopic point of view, these organized structures result in a compact morphology (Fig. 5D) with some elongated particles that could be due to the presence of biotin units on the coating surface as reported elsewhere for other biotinylated nanomaterials [61].

Layer-by-layer (LbL) self-assembly technique [68] has been explored to fabricate multilayered structures that could not only improve the biomolecules loading but were also capable of maintaining the optimum biochemical activity.

Interestingly the biotin-avidin binding ability of the PDA-BT (10 mM) coating was hold on even after alternated immersion in freshly prepared HABA/Avidin and biotin solutions. After four cycles of avidin/biotin dipping, the absorbance decay at 505 nm did not change much

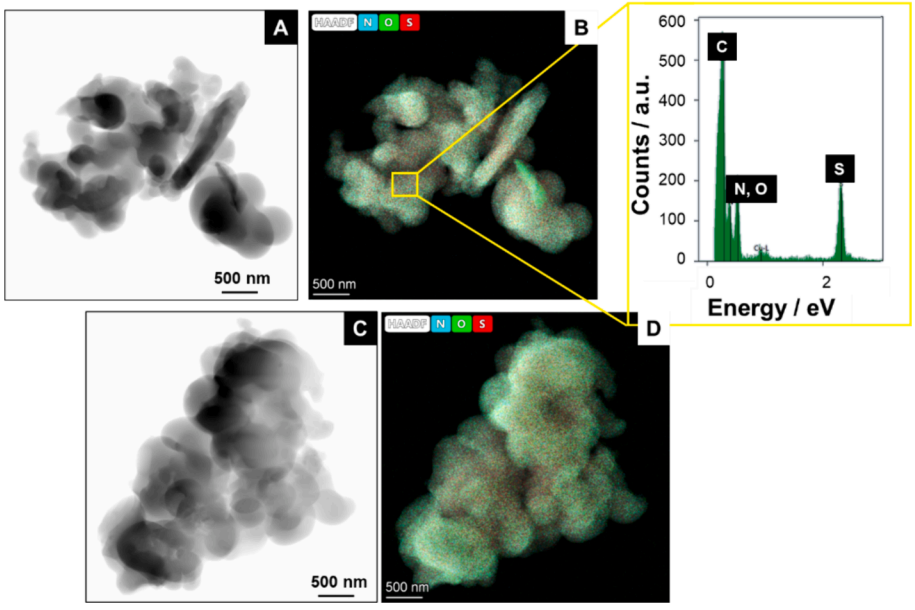

Fig. 3. HAADF/STEM images of (A-B) PDA-BT coating obtained from DA-BT 5 mM and its elemental mapping; the inset shows the EDX spectrum of the selected area; (C-D) PDA-BT obtained from DA-BT 10 mM.

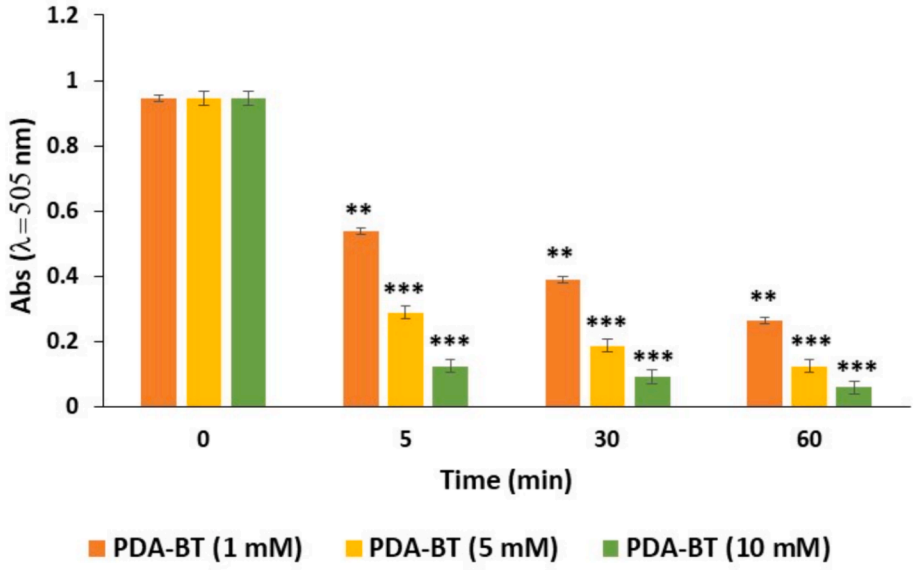

Fig. 4. Kinetics of decay of HABA/Avidin complex absorption maximum at a selected wavelength (505 nm). Reported are the mean ± SD values of three experiments. Significance is given for each coating at the selected times *versus* the initial HAVA/Avidin complex absorbance (time 0). ** $p < 0.05$, *** $p < 0.01$.

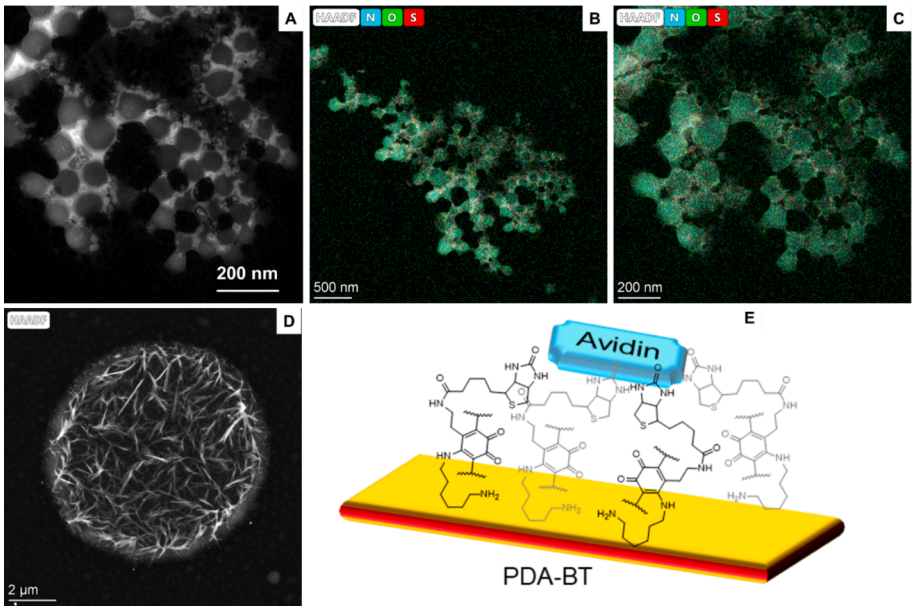

Fig. 5. (A-D) HAADF/STEM images of PDA-BT coating obtained from DA-BT 5 mM treated with HABA/Avidin solution; (E) possible hypothesized interaction among the different biotin units of the PDA-BT coating and avidin.

compared with the initial state suggesting that the film is still active (Fig. S6).

The films undergo a morphology change from particle like for the PDA-BT deposition to a mixture of particles and small needles (about 1 μm long) after one deposition cycle to extremely long and broad needles (more than 20 μm long and a few μm broad) after 8 deposition cycles (Fig. 6b). This suggests an ordered self-assembly process which will be investigated in upcoming studies. Furthermore, PDA-BT coating exhibited a relatively high water-contact angle (WCA) of about 64.7 ± 0.4° indicating a moderate hydrophilic character that lowered to 59.8 ± 0.5° after 1 h interaction with avidin. After sequential immersion in biotin and avidin solutions, the WCA value of the PDA-BT coating significantly decreased to 33.1 ± 0.7°, suggesting an increase in hydrophilicity likely due to specific biotin-avidin interaction. This marked decrease in WCA after LbL deposition could also be due to an increased surface roughness in relation to the needle morphology (Fig. 6B).

3.2. Cancer cell recognition

Accurate differentiation of cancer cell types at a molecular level is highly desirable for diagnostic and therapeutic purposes.

To investigate the feasibility of PDA-BT (10 mM) coating to recognize cell lines with different grade of overexpression of biotin receptors (BR), a tumor cell capture experiment was performed on a glass slide, or PDA coating glass slide, as negative controls, or on PDA-BT coating on a glass slide, using BR(+) and BR(−) cancer cell lines. In particular, the BR (+) MCF-7 cell lines [69] and the BR(−) HL-60 ones, where chosen as model.

In the experimental conditions adopted no toxicity of the PDA-coating was detected.

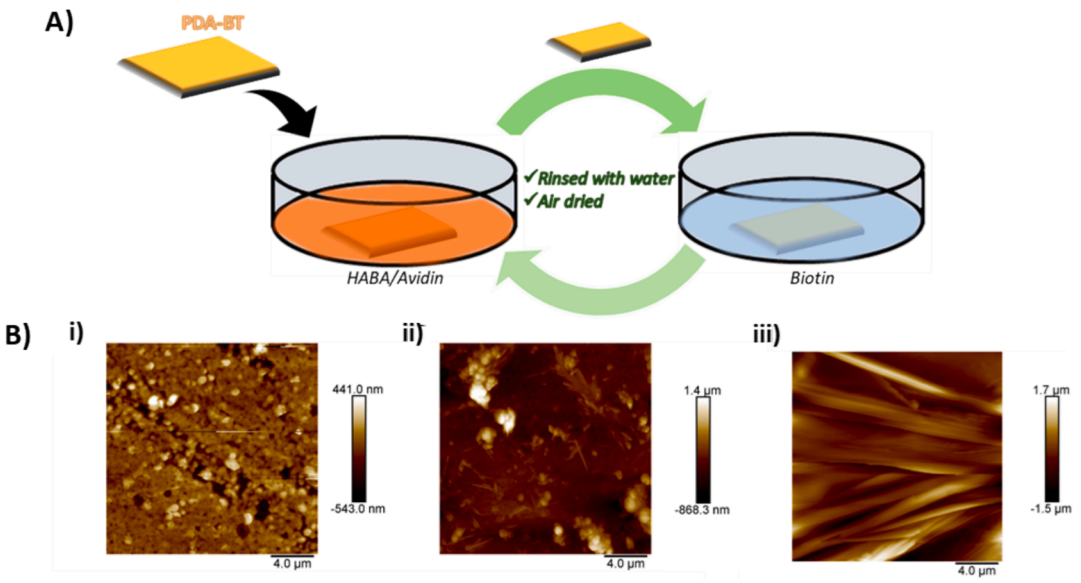

Fig. 6. (A) Schematic representation of the LbL avidin–biotin deposition. (B) AFM topographies (20 µm × 20 µm) of i): the PDA-BT film (RMS roughness: 112 nm), ii): the same with one deposition cycle of avidin (RMS roughness: 271 nm) and iii) after 8 deposition cycles (RMS roughness: 412 nm).

Fig. 7A–C show the DAPI-staining fluorescence images of captured MCF-7 cells on glass slide (Fig. 7A), PDA (Fig. 7B) and PDA-BT (Fig. 7C) coating glass slides. As it is possible to observe, the captured cell number on the PDA-BT coating is much higher compared to both blank glass slide and PDA coating further confirming the presence of biotin units exposed at the surface of PDA-BT coating, exerting their receptor-binding ability. On the contrary, as shown in Fig. 7D–E, a very low amount of HL-60 cells was captured by the film showing thus, the PDA-BT coating developed in this study can selectively recognize cancer cells showing an high expression of biotin receptors on their surface.

The number of cells captured on the same areas of different surfaces was counted to quantify the capture efficiency and the obtained results are reported in Fig. 7F.

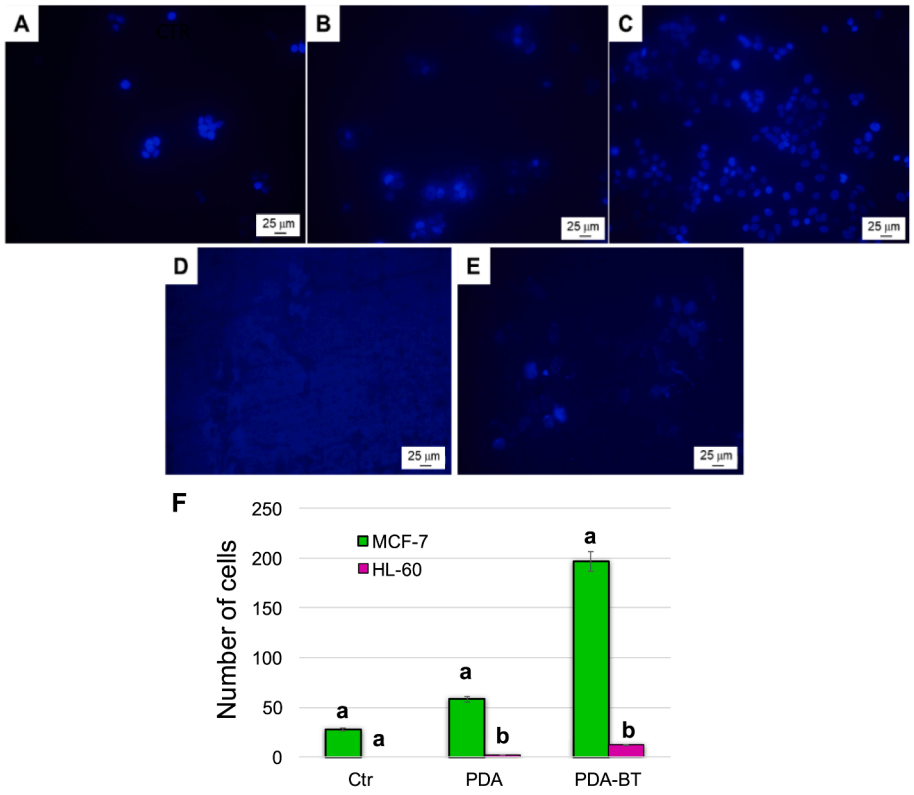

Fig. 7. The DAPI fluorescence microscopy images of captured cells of MCF-7 (A–C) and HL-60 (D–E) cells on (A, D) blank glass; (B) PDA coating glass, (C, E) PDA-BT coating glass; (F) number of cells captured on the different glass substrates. Image captured under fluorescence microscope (20×). Scale bar: 25 µm. In the graph, different letters above the columns indicate significant differences ($p < 0.05$).

4. Conclusions

In conclusion, an easily accessible, low cost and recyclable biosensor with the dual and rapid detection of both proteins and cells was developed. To achieve this objective, firstly, *N*-biotinyl-(3,4-dihydroxyphenylethylamide) (DA-BT) was synthetized by an EDC mediated condensation between dopamine hydrochloride and biotin. Then, the synthetized DA-BT was used as monomer to obtain the final PDA-BT film. Since autoxidation of DA-BT did not lead to any appreciable polymerization, the latter was performed in the presence of hexamethylenediamine in carbonate buffer at pH 9.0, which results in the deposition of a yellowish-orange thin film on a series of different materials ranging from quartz or plastic surfaces to porous aluminum oxide particles. The best experimental conditions, in terms of DA-BT concentration, were investigated by UV–*vis* spectroscopy.

The structural features of the PDA-BT films were studied by ^{13}C NMR solid state spectroscopy performed, for the first time, on the film deposited onto alumina spheres. This technique confirmed the presence of biotin in the final film exposed onto the coating surface, as well as the successful incorporation of HMDA into it. Morphological characterization by HAADF/STEM coupled with EDX showed the presence of a compact structure and round shaped particles typical of polydopamine as also confirmed by AFM measurements. The receptor binding capacity of the PDA-BT coating toward 4-hydroxyazobenzene-2-carboxylic acid (HABA)/Avidin complex was also verified by means of UV–*vis* spectroscopy. By dipping the PDA-BT film into the HABA/Avidin solution, a decrease in the absorption maximum band of the complex was observed consistent with displacement of HABA molecules from the avidin complex; in particular *ca.* 87 % reduction of HABA/Avidin absorption maximun in the first 5 min was achieved. Different deposition cycles of avidin onto the PDA-BT coating by layer-by-layer assembly showed that the film retains its receptor binding capacity for at least eight consecutive cycles as also verified by water contact angle measurements and morphological investigations. Finally, the feasibility of PDA-BT coating to recognize cell lines with different grade of overexpression of biotin receptors (BR) was investigated by a tumor cell capture experiment by using MCF-7 (BR+) and HL-60 (BR−) cell lines. The study indicates that the developed film is able to selectively capture MCF-7 cells over the HL-60 ones. Thus, the development of PDA-biotin technology could represent an attractive choice for potential applications in different areas of material functionalization, biomedical imaging and pharmacology.

Author contributions

The manuscript was written through contributions of all authors. All authors have given approval to the final version of the manuscript.

CRediT authorship contribution statement

Monica Notarbartolo: Writing – review & editing, Writing – original draft, Methodology, Investigation. **Maria Laura Alfieri:** Writing – review & editing, Writing – original draft, Methodology, Investigation, Conceptualization. **Roberto Avolio:** Writing – original draft, Methodology, Investigation. **Vincent Ball:** Writing – original draft, Methodology, Investigation. **Maria Emanuela Errico:** Writing – original draft, Methodology, Investigation. **Marina Massaro:** Writing – review & editing, Writing – original draft, Methodology, Investigation, Conceptualization. **Roberta Puglisi:** Methodology, Investigation. **Rita Sànchez-Espejo:** Methodology, Investigation. **César Viseras:** Resources, Methodology, Investigation. **Serena Riela:** Writing – review & editing, Writing – original draft, Methodology, Investigation.

Declaration of competing interest

The authors declare that they have no known competing financial interests or personal relationships that could have appeared to influence the work reported in this paper.

Data availability

Data will be made available on request.

Acknowledgements

This work was supported by PJ_UTILE_2022VQR_Misura_B_D15_Notarbartolo of University of Palermo.

Appendix A. Supplementary data

Supplementary data (^{1}H and ^{13}C NMR spectra of DA-BT; AFM image of PDA-BT film; kinetic of decay of HABA/Avidin complex absorption maximum; UV–*vis* spectra and of changes of absorbance at 505 nm of PDA-BT coating before and after dipping in HABA-Avidin solution) to this article can be found online at https://doi.org/10.1016/j.jcis.2024.09.145.

References

[1] J. Lu, L. Song, S. Feng, K. Wang, Y. Mao, Y. Gao, Q. Zhao, S. Wang, Nanozyme-mediated biocatalysis as a mitochondrial oxidative stress amplifier for tumor nanocatalytic immunotherapy, Chem. Eng. J. 481 (2024) 148270, https://doi.org/10.1016/J.CEJ.2023.148270.

[2] Y. Su, Q. Tian, D. Pan, L. Hui, Y. Chen, Q. Zhang, W. Tian, J. Yu, S. Hu, Y. Gao, D. Qian, T. Xie, B. Wang, Antibody-functional microsphere-integrated filter chip with inertial microflow for size-immune-capturing and digital detection of circulating tumor cells, ACS Appl. Mater. Interfaces 11 (2019) 29569–29578, https://doi.org/10.1021/ACSAMI.9B09655.

[3] S. Asghari, M. Mahmoudifard, Core-shell nanofibrous membrane of polycaprolactone-hyaluronic acid as a promising platform for the efficient capture and release of circulating tumor cells, Polym. Adv. Technol. 32 (2021) 1101–1113, https://doi.org/10.1002/PAT.5158.

[4] A. Pramanik, S. Jones, Y. Gao, C. Sweet, A. Vangara, S. Begum, P.C. Ray, Multifunctional hybrid graphene oxide for circulating tumor cell isolation and analysis, Adv. Drug Deliv. Rev. 125 (2018) 21–35, https://doi.org/10.1016/J.ADDR.2018.01.004.

[5] H. Cui, Q. Liu, R. Li, X. Wei, Y. Sun, Z. Wang, L. Zhang, X.Z. Zhao, B. Hua, S.S. Guo, ZnO nanowire-integrated bio-microchips for specific capture and non-destructive release of circulating tumor cells, Nanoscale 12 (2020) 1455–1463, https://doi.org/10.1039/C9NR07349C.

[6] J. Chen, L. Yu, Y. Li, J.L. Cuellar-Camacho, Y. Chai, D. Li, Y. Li, H. Liu, L. Ou, W. Li, R. Haag, Biospecific monolayer coating for multivalent capture of circulating tumor cells with high sensitivity, Adv. Funct. Mater. 29 (2019) 1808961, https://doi.org/10.1002/ADFM.201808961.

[7] R. Li, F.F. Chen, H.Q. Liu, Z.X. Wang, Z.T. Zhang, Y. Wang, H. Cui, W. Liu, X. Z. Zhao, Z.J. Sun, S.S. Guo, Efficient capture and high activity release of circulating tumor cells by using TiO_2 nanorod arrays coated with soluble MnO_2 nanoparticles, ACS Appl. Mater. Interfaces 10 (2018) 16327–16334, https://doi.org/10.1021/ACSAMI.8B04683.

[8] Z. Wang, Z. Wu, N. Sun, Y. Cao, X. Cai, F. Yuan, H. Zou, C. Xing, R. Pei, Antifouling hydrogel-coated magnetic nanoparticles for selective isolation and recovery of circulating tumor cells, J. Mater. Chem. B 9 (2021) 677–682, https://doi.org/10.1039/D0TB02380A.

[9] C. Liu, B. Yang, X. Chen, Z. Hu, Z. Dai, D. Yang, X. Zheng, X. She, Q. Liu, Capture and separation of circulating tumor cells using functionalized magnetic nanocomposites with simultaneous in situ chemotherapy, Nanotechnology 30 (2019) 285706, https://doi.org/10.1088/1361-6528/AB0E25.

[10] S. Siemer, D. Wünsch, A. Khamis, Q. Lu, A. Scherberich, M. Filippi, M.P. Krafft, J. Hagemann, C. Weiss, G. Bin Ding, R.H. Stauber, A. Gribko, Nano meets micro-translational nanotechnology in medicine: nano-based applications for early tumor detection and therapy, Nanomaterials 10 (2020) 383, https://doi.org/10.3390/NANO10020383.

[11] K. Niciński, J. Krajczewski, A. Kudelski, E. Witkowska, J. Trzcińska-Danielewicz, A. Girstun, A. Kamińska, Detection of circulating tumor cells in blood by shell-isolated nanoparticle – enhanced Raman spectroscopy (SHINERS) in microfluidic device, Sci. Rep. 9 (2019) 1–14, https://doi.org/10.1038/s41598-019-45629-7.

[12] Y. Liu, R. Li, L. Zhang, S. Guo, Nanomaterial-based immunocapture platforms for the recognition, isolation, and detection of circulating tumor cells, Front. Bioeng. Biotechnol. 10 (2022) 850241, https://doi.org/10.3389/FBIOE.2022.850241.

[13] D. Zou, D. Cui, Advances in isolation and detection of circulating tumor cells based on microfluidics, Cancer Biol. Med. 15 (2018) 335, https://doi.org/10.20892/J.ISSN.2095-3941.2018.0256.

[14] S. Ju, C. Chen, J. Zhang, L. Xu, X. Zhang, Z. Li, Y. Chen, J. Zhou, F. Ji, L. Wang, Detection of circulating tumor cells: opportunities and challenges, Biomark. Res. 10 (2022) 1–25, https://doi.org/10.1186/S40364-022-00403-2.

[15] W. Li, E. Reátegui, M.H. Park, S. Castleberry, J.Z. Deng, B. Hsu, S. Mayner, A. E. Jensen, L.V. Sequist, S. Maheswaran, D.A. Haber, M. Toner, S.L. Stott, P. T. Hammond, Biodegradable nano-films for capture and non-invasive release of circulating tumor cells, Biomaterials 65 (2015) 93–102, https://doi.org/10.1016/J.BIOMATERIALS.2015.06.036.
[16] E.P. Kaldjian, A.B. Ramirez, L. Costandy, N.G. Ericson, W.I. Malkawi, T.C. George, P.M. Kasi, Beyond circulating tumor cell enumeration: cell-based liquid biopsy to assess protein biomarkers and cancer genomics using the RareCyte® Platform, Front. Pharmacol. 13 (2022) 835727, https://doi.org/10.3389/FPHAR.2022.835727.
[17] Y. Foelen, R. Puglisi, M.G. Debije, A.P.H.J. Schenning, Photonic liquid crystal polymer absorbent for immobilization and detection of gaseous nerve agent simulants, ACS Appl. Opt. Mater. 1 (2023) 107–114, https://doi.org/10.1021/acsaom.2c00014.
[18] M. Vidlarova, A. Rehulkova, P. Stejskal, A. Prokopova, H. Slavik, M. Hajduch, J. Srovnal, Recent advances in methods for circulating tumor cell detection, Int. J. Mol. Sci. 24 (2023) 3902, https://doi.org/10.3390/IJMS24043902.
[19] Y. Zhang, X. Kong, M. Li, Y. Yin, W. Lin, The development of a biotin-guided and mitochondria-targeting fluorescent probe for detecting SO_2 precisely in cancer cells, Talanta 225 (2021) 121992, https://doi.org/10.1016/J.TALANTA.2020.121992.
[20] K. Li, J.T. Hou, J. Yang, X.Q. Yu, A tumor-specific and mitochondria-targeted fluorescent probe for real-time sensing of hypochlorite in living cells, Chem. Commun. 53 (2017) 5539–5541, https://doi.org/10.1039/C7CC01679D.
[21] A. Doerflinger, N.N. Quang, E. Gravel, G. Pinna, M. Vandamme, F. Ducongé, E. Doris, Biotin-functionalized targeted polydiacetylene micelles, Chem. Commun. 54 (2018) 3613–3616, https://doi.org/10.1039/C8CC00553B.
[22] A.D. Vadlapudi, R.K. Vadlapatla, D. Pal, A.K. Mitra, Biotin uptake by T47D breast cancer cells: Functional and molecular evidence of sodium-dependent multivitamin transporter (SMVT), Int. J. Pharm. 441 (2013) 535–543, https://doi.org/10.1016/J.IJPHARM.2012.10.047.
[23] L. Bu, L.C. Gan, X.Q. Guo, F.Z. Chen, Q. Song, Q. Zhao, X.J. Gou, S.X. Hou, Q. Yao, Trans-resveratrol loaded chitosan nanoparticles modified with biotin and avidin to target hepatic carcinoma, Int. J. Pharm. 452 (2013) 355–362, https://doi.org/10.1016/J.IJPHARM.2013.05.007.
[24] D. Li, X.Z. Wang, L.F. Yang, S.C. Li, Q.Y. Hu, X. Li, B.Y. Zheng, M.R. Ke, J.D. Huang, Size-tunable targeting-triggered nanophotosensitizers based on self-assembly of a phthalocyanine-biotin conjugate for photodynamic therapy, ACS Appl. Mater. Interfaces 11 (2019) 36435–36443, https://doi.org/10.1021/ACSAMI.9B13861.
[25] W.X. Ren, J. Han, S. Uhm, Y.J. Jang, C. Kang, J.H. Kim, J.S. Kim, Recent development of biotin conjugation in biological imaging, sensing, and target delivery, Chem. Comm. 51 (2015) 10403–10418, https://doi.org/10.1039/C5CC03075G.
[26] J.F. Shi, P. Wu, Z.H. Jiang, X.Y. Wei, Synthesis and tumor cell growth inhibitory activity of biotinylated annonaceous acetogenins, Eur. J. Med. Chem. 71 (2014) 219–228, https://doi.org/10.1016/J.EJMECH.2013.11.012.
[27] H. Shi, N. Liang, J. Liu, S. Li, X. Gong, P. Yan, S. Sun, AIE-active polymeric micelles based on modified chitosan for bioimaging-guided targeted delivery and controlled release of paclitaxel, Carbohydr. Polym. 269 (2021) 118327, https://doi.org/10.1016/J.CARBPOL.2021.118327.
[28] W. Yang, M. Wang, L. Ma, H. Li, L. Huang, Synthesis and characterization of biotin modified cholesteryl pullulan as a novel anticancer drug carrier, Carbohydr. Polym. 99 (2014) 720–727, https://doi.org/10.1016/J.CARBPOL.2013.09.013.
[29] X.Q. Dou, J. Zhang, C. Feng, Biotin-avidin based universal cell-matrix interaction for promoting three-dimensional cell adhesion, ACS Appl. Mater. Interfaces 7 (2015) 20786–20792, https://doi.org/10.1021/ACSAMI.5B05828.
[30] N.N. Lu, M. Xie, J. Wang, S.W. Lv, J.S. Yi, W.G. Dong, W.H. Huang, Biotin-triggered decomposable immunomagnetic beads for capture and release of circulating tumor cells, ACS Appl. Mater. Interfaces 7 (2015) 8817–8826, https://doi.org/10.1021/ACSAMI.5B01397.
[31] N. Shirasu, H. Shibaguchi, H. Yamada, M. Kuroki, S. Yasunaga, Highly versatile cancer photoimmunotherapy using photosensitizer-conjugated avidin and biotin-conjugated targeting antibodies, Cancer Cell Int. 19 (2019) 1–13, https://doi.org/10.1186/S12935-019-1034-4.
[32] M. Massaro, P. Poma, G. Cavallaro, F. García-Villén, G. Lazzara, M. Notarbartolo, N. Muratore, R. Sánchez-Espejo, C. Viseras Iborra, S. Riela, Prodrug based on halloysite delivery systems to improve the antitumor ability of methotrexate in leukemia cell lines, Colloids Surf., B Biointerfaces 213 (2022) 112385. doi: 10.1016/J.COLSURFB.2022.112385.
[33] M. Xu, S. Asghar, S. Dai, Y. Wang, S. Feng, L. Jin, F. Shao, Y. Xiao, Mesenchymal stem cells-curcumin loaded chitosan nanoparticles hybrid vectors for tumor-tropic therapy, Int. J. Biol. Macromol. 134 (2019) 1002–1012, https://doi.org/10.1016/J.IJBIOMAC.2019.04.201.
[34] C.F. de Freitas, M.C. Montanha, D.S. Pellosi, E. Kimura, W. Caetano, N. Hioka, Biotin-targeted mixed liposomes: a smart strategy for selective release of a photosensitizer agent in cancer cells, Mater. Sci. Eng. C 104 (2019) 109923, https://doi.org/10.1016/J.MSEC.2019.109923.
[35] J.H.T. Luong, K.B. Male, J.D. Glennon, Biotin interference in immunoassays based on biotin-strept(avidin) chemistry: an emerging threat, Biotechnol. Adv. 37 (2019) 634–641, https://doi.org/10.1016/J.BIOTECHADV.2019.03.007.
[36] N.U. Deshpande, M. Jayakannan, Biotin-tagged polysaccharide vesicular nanocarriers for receptor-mediated anticancer drug delivery in cancer cells, Biomacromolecules 19 (2018) 3572–3585, https://doi.org/10.1021/ACS.BIOMAC.8B00833.
[37] Z. Chai, D. Ran, L. Lu, C. Zhan, H. Ruan, X. Hu, C. Xie, K. Jiang, J. Li, J. Zhou, J. Wang, Y. Zhang, R.H. Fang, L. Zhang, W. Lu, Ligand-modified cell membrane enables the targeted delivery of drug nanocrystals to glioma, ACS Nano 13 (2019) 5591–5601, https://doi.org/10.1021/ACSNANO.9B00661.
[38] E.B. Lurier, V.A. Nash, H.S. Abee, T.B. Wissing, C.V.C. Bouten, A.I.P.M. Smits, K. L. Spiller, Imparting immunomodulatory activity to scaffolds via biotin-avidin interactions, ACS Biomater Sci. Eng. 7 (2021) 5611–5621, https://doi.org/10.1021/ACSBIOMATERIALS.1C01190.
[39] P. Henke, J. Dolanský, P. Kubát, J. Mosinger, Multifunctional photosensitizing and biotinylated polystyrene nanofiber membranes/composites for binding of biologically active compounds, ACS Appl. Mater. Interfaces 12 (2020) 18792–18802, https://doi.org/10.1021/ACSAMI.9B23104.
[40] S. Wang, M.Z. Hossain, T. Han, K. Shinozuka, T. Suzuki, A. Kuwana, H. Kobayashi, Avidin−biotin technology in gold nanoparticle-decorated graphene field effect transistors for detection of biotinylated macromolecules with ultrahigh sensitivity and specificity, ACS Omega 5 (2020) 30037–30046, https://doi.org/10.1021/ACSOMEGA.0C04429.
[41] D. Deng, X. Li, J.J. Zhang, Y. Yin, Y. Tian, D. Gan, R. Wu, J. Wang, B.M. Tian, F. M. Chen, X.T. He, Biotin-avidin system-based delivery enhances the therapeutic performance of MSC-derived exosomes, ACS Nano 17 (2023) 8530–8550, https://doi.org/10.1021/ACSNANO.3C00839.
[42] H. Feinberg, T.W. Hanks, Polydopamine: a bioinspired adhesive and surface modification platform, Polym. Int. 71 (2022) 578–582, https://doi.org/10.1002/PI.6358.
[43] S. Cai, Y. Cheng, C. Qiu, G. Liu, C. Chu, The versatile applications of polydopamine in regenerative medicine: progress and challenges, Smart. Mater. Med. 4 (2023) 294–312, https://doi.org/10.1016/J.SMAIM.2022.11.005.
[44] M.K. Yazdi, M. Zare, A. Khodadadi, F. Seidi, S.M. Sajadi, P. Zarrintaj, A. Arefi, M. R. Saeb, M. Mozafari, Polydopamine biomaterials for skin regeneration, ACS Biomater Sci. Eng. 8 (2022) 2196–2219, https://doi.org/10.1021/ACSBIOMATERIALS.1C01436.
[45] H. Xu, Y. Zhang, H. Zhang, Y. Zhang, Q. Xu, J. Lu, S. Feng, X. Luo, S. Wang, Q. Zhao, Smart polydopamine-based nanoplatforms for biomedical applications: state-of-art and further perspectives, Coord. Chem. Rev. 488 (2023) 215153, https://doi.org/10.1016/J.CCR.2023.215153.
[46] J.H. Ryu, P.B. Messersmith, H. Lee, Polydopamine surface chemistry: a decade of discovery, ACS Appl. Mater. Interfaces 10 (2018) 7523–7540, https://doi.org/10.1021/ACSAMI.7B19865.
[47] M.L. Alfieri, T. Weil, D.Y.W. Ng, V. Ball, Polydopamine at biological interfaces, Adv. Colloid Interface Sci. 305 (2022) 102689, https://doi.org/10.1016/J.CIS.2022.102689.
[48] S. El Yakhlifi, V. Ball, Polydopamine as a stable and functional nanomaterial, Colloids Surf. B Biointerfaces 186 (2020) 110719, https://doi.org/10.1016/J.COLSURFB.2019.110719.
[49] S. Li, J.M. Scheiger, Z. Wang, Z. Dong, A. Welle, V. Trouillet, P.A. Levkin, Substrate-independent and re-writable surface patterning by combining polydopamine coatings, silanization, and thiol-Ene reaction, Adv. Funct. Mater. 31 (2021) 2107716, https://doi.org/10.1002/ADFM.202107716.
[50] Y. Li, Y. Cheng, Y. Wu, Z. Wang, X. Ma, J. Zhao, Z. Yang, Y. Ji, Polydopamine-coated self-assembled lipid nanoparticles for highly effective chemo-photothermal combination therapy, Ind. Eng. Chem. Res. 63 (2024) 3140–3151, https://doi.org/10.1021/ACS.IECR.3C04310.
[51] T. Ding, Y. Xing, Z. Wang, H. Guan, L. Wang, J. Zhang, K. Cai, Structural complementarity from DNA for directing two-dimensional polydopamine nanomaterials with biomedical applications, Nanoscale Horiz. 4 (2019) 652–657, https://doi.org/10.1039/C8NH00351C.
[52] M.L. Alfieri, L. Panzella, A. Napolitano, Multifunctional coatings hinging on the catechol/amine interplay, E. J. Org. Chem. 27 (2024) e202301002, https://doi.org/10.1002/EJOC.202301002.
[53] S. Hong, Y. Wang, S.Y. Park, H. Lee, Progressive fuzzy cation- assembly of biological catecholamines, Sci. Adv. 4 (2018) 7457–7464, https://doi.org/10.1126/SCIADV.AAT7457.
[54] S. Hong, Y.S. Na, S. Choi, I.T. Song, W.Y. Kim, H. Lee, Non-covalent self-assembly and covalent polymerization co-contribute to polydopamine formation, Adv. Funct. Mater. 22 (2012) 4711–4717, https://doi.org/10.1002/ADFM.201201156.
[55] M.L. Alfieri, R. Micillo, L. Panzella, O. Crescenzi, S.L. Oscurato, P. Maddalena, A. Napolitano, V. Ball, M. d'Ischia, Structural basis of polydopamine film formation: probing 5,6-dihydroxyindole-based eumelanin type units and the porphyrin issue, ACS Appl. Mater. Interfaces 10 (2018) 7670–7680, https://doi.org/10.1021/ACSAMI.7B09662.
[56] H. Safari Yazd, Y. Yang, L. Li, L. Yang, X. Li, X. Pan, Z. Chen, J. Jiang, C. Cui, W. Tan, Precise deposition of polydopamine on cancer cell membrane as artificial receptor for targeted drug delivery, iScience 23 (2020) 101750. doi: 10.1016/J.ISCI.2020.101750.
[57] H. Cao, B. Jiang, Y. Yang, M. Zhao, N. Sun, J. Xia, X. Gao, J. Li, Cell membrane covered polydopamine nanoparticles with two-photon absorption for precise photothermal therapy of cancer, J. Colloid Interface Sci. 604 (2021) 596–603, https://doi.org/10.1016/J.JCIS.2021.07.004.
[58] M. Li, Y. Xuan, W. Zhang, S. Zhang, J. An, Polydopamine-containing nano-systems for cancer multi-mode diagnoses and therapies: a review, Int. J. Biol. Macromol. 247 (2023) 125826, https://doi.org/10.1016/J.IJBIOMAC.2023.125826.
[59] T.T. Zheng, R. Zhang, L. Zou, J.J. Zhu, A label-free cytosensor for the enhanced electrochemical detection of cancer cells using polydopamine-coated carbon nanotubes, Analyst 137 (2012) 1316–1318, https://doi.org/10.1039/C2AN16023D.
[60] J. Liu, L. Kang, S. Smith, C. Wang, Transmembrane MUC18 targeted polydopamine nanoparticles and a mild photothermal effect synergistically disrupt actin

cytoskeleton and migration of cancer cells, Nano Lett. 21 (2021) 9609–9618, https://doi.org/10.1021/ACS.NANOLETT.1C03377.
[61] M.L. Alfieri, M. Massaro, M. d'Ischia, G. D'Errico, N. Gallucci, M. Gruttadauria, M. Licciardi, L.F. Liotta, G. Nicotra, G. Sfuncia, S. Riela, Site-specific halloysite functionalization by polydopamine: a new synthetic route for potential near infrared-activated delivery system, J. Colloid Interface Sci. 606 (2022) 1779–1791, https://doi.org/10.1016/J.JCIS.2021.08.155.
[62] Y. Wan, G. Zhu, Dopamine-mediated immunoassay for bacteria detection, Anal. Bioanal. Chem. 409 (2017) 6091–6096, https://doi.org/10.1007/S00216-017-0545-X.
[63] M.L. Alfieri, G. Riccucci, S. Ferraris, A. Cochis, A.C. Scalia, L. Rimondini, L. Panzella, S. Spriano, A. Napolitano, Deposition of antioxidant and cytocompatible caffeic acid-based thin films onto Ti6Al4V alloys through hexamethylenediamine-mediated crosslinking, ACS Appl. Mater. Interfaces 15 (2023) 29618–29635, https://doi.org/10.1021/ACSAMI.3C05564.
[64] M.L. Alfieri, L. Panzella, S.L. Oscurato, M. Salvatore, R. Avolio, M.E. Errico, P. Maddalena, A. Napolitano, V. Ball, M. d'Ischia, Hexamethylenediamine-mediated polydopamine film deposition: Inhibition by resorcinol as a strategy for mapping quinone targeting mechanisms, Front. Chem. 7 (2019) 465661, https://doi.org/10.3389/FCHEM.2019.00407.
[65] R. Argenziano, M.L. Alfieri, Y. Arntz, R. Castaldo, D. Liberti, D. Maria Monti, G. Gentile, L. Panzella, O. Crescenzi, V. Ball, A. Napolitano, M. d'Ischia, Non-covalent small molecule partnership for redox-active films: beyond polydopamine technology, J. Colloid Interface Sci. 624 (2022) 400–410. doi: 10.1016/J.JCIS.2022.05.123.
[66] S. Chen, J. Zhang, Y. Chen, S. Zhao, M. Chen, X. Li, M.F. Maitz, J. Wang, N. Huang, Application of phenol/amine copolymerized film modified magnesium alloys: anticorrosion and surface biofunctionalization, ACS Appl. Mater. Interfaces 7 (2015) 24510–24522, https://doi.org/10.1021/ACSAMI.5B05851.
[67] M.L. Alfieri, L. Panzella, S.L. Oscurato, M. Salvatore, R. Avolio, M.E. Errico, P. Maddalena, A. Napolitano, M. d'Ischia, The chemistry of polydopamine film formation: the amine-quinone interplay, Biomimetics 3 (2018) 26, https://doi.org/10.3390/BIOMIMETICS3030026.
[68] G. Decher, Fuzzy nanoassemblies: toward layered polymeric multicomposites, Science (1979) 277 (1997) 1232–1237, https://doi.org/10.1126/SCIENCE.277.5330.1232.
[69] B. Bertrand, M.A. O'Connell, Z.A.E. Waller, M. Bochmann, A gold(III) pincer ligand scaffold for the synthesis of binuclear and bioconjugated complexes: synthesis and anticancer potential, Chem. Eur. J. 24 (2018) 3613–3622, https://doi.org/10.1002/CHEM.201705902.